Experimental and modeling investigation of partial oxidation of gasification tars

Rémi Demol, Miguel Ruiz, Adam Schnitzer, Olivier Herbinet, Guillain Mauviel

Experimental and Modeling Investigation of Partial Oxidation of Gasification Tars

Rémi DEMOL[1], Miguel RUIZ[1], Adam SCHNITZER[1], Olivier HERBINET[1], Guillain MAUVIEL[1,*].

1. Université de Lorraine, CNRS, Fédération J. Villermaux, F-54000, Nancy, France.

*Corresponding author: guillain.mauviel@univ-lorraine.fr (G. Mauviel)

Published in Fuel (doi.org/10.1016/j.fuel.2023.128990).

GRAPHICAL ABSTRACT

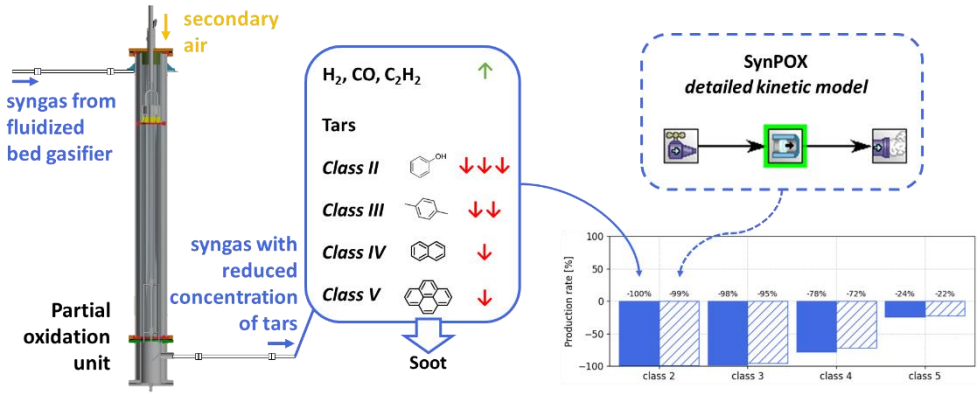

HIGHLIGHTS

- Fluidized bed gasifier and partial oxidation unit coupled at pilot-scale.
- Detailed kinetic model developed including heavy tars and soot formation.
- Comparison between experiments and model predictions.
- An equivalence ratio of 0.10 for secondary air recommended to reduced 90% of tars.

ABSTRACT

Among the methods to reduce tar emission, the partial oxidation (POX) of biomass gasification tars has been studied both experimentally at a pilot-scale and numerically. The gasification producer gas was obtained at a temperature of 800°C in an air-blown fluidized bed with an equivalent ratio (ER) of 0.25. For the POX unit, two secondary ER values were selected: 0.05 and 0.10, with the option of pre-heating air or not. Multiple advanced analytical methods were employed to provide a detailed composition of the producer gas, tars and acid gases. The POX unit demonstrated the ability to reduce tar levels by 60 to 90% depending on the secondary ER (from 6.5 to 2.4 and 0.72 g_{tars}/Nm^3, excluding benzene). The lighter tars were almost completely eliminated. The permanent gases were barely modified while the light hydrocarbons (except C_2H_2) and benzene were significantly reduced. Consequently, there was a slight decrease in the lower heating value. These results were compared to an isothermal plug flow reactor model, which utilized a detailed radical kinetic scheme constructed from various sources to account for all the species measured during the experiments as well as soot mass yield. The model provided relatively accurate predictions of the hydrocarbon species variations, even though it did not consider the mixing between air and syngas at the inlet of the POX unit.

KEYWORDS

Biomass gasification, Tars, Partial oxidation, Detailed kinetic model.

1. INTRODUCTION

Biomass has been utilized for centuries as a heat source and material [1]. Currently, there is a growing interest in using biomass as a substitute for fossil fuels in the production of energy and chemicals.

Pyrogasification processes offer a way to produce these bio-based products. With a limited amount of oxygen, gasification produces a synthetic gas mainly composed of H_2, CO, CO_2, CH_4 and lights hydrocarbons (C_2+). This technology is commercially viable for energy production (power and heat). However, a portion of the solid fuel remains in the syngas as simple aromatics (BTX) and polycyclic aromatic hydrocarbons (PAHs), which pose challenges to the overall process due to the risk of clogging downstream equipment. Additionally, the handling of tar sludge after capture is complex and costly. Tar removal is also necessary for various applications of syngas, such as gas engines, gas turbines, Fischer-Tropsch processes, and H2 recovery [2,3]. Moreover, the release of these compounds into the atmosphere is environmentally harmful, with sixteen of these PAHs classified as priority pollutants by the United States Environmental Protection Agency [4].

Over the past few decades, several physical, chemical and catalytic cleanup strategies have been developed [2]. These methods are classified as primary or secondary based on their application location. Primary methods aim to prevent tar formation inside the reactor through reactor technology, optimization of the gasification parameters, gasifying agent and fluidized bed media. The addition of alkali and alkaline earth metal species during gasification can reduce tar production [5]. Secondary methods focus on eliminating tars after the gasifier, using high, mild or low-temperatures techniques, either in a dry or wet process [2,6]. Generally, a combination of primary and secondary methods is required to meet quality standards.

The secondary elimination of gasification tars can occur through three cracking modes at elevated temperatures. Thermal cracking involves the pyrolytic decomposition of tar molecules in the gas phase at high temperature (>900°C) without catalyst and under inert atmosphere. Numerous studies have explored the mechanisms and kinetics of thermal cracking of tars, focusing on pyrolysis vapors (Table 1) and model molecules derived from primary and secondary tars from the pyrolysis reaction, such as benzene, catechol,

toluene, naphthalene. However, less information is available regarding the thermal decomposition of tertiary tars typically present in producer gas, specifically refractory PAHs. Furthermore, implementing thermal cracking at an industrial scale is challenging due to heat transfer difficulties and the negative impact of the external energy required to achieve cracking temperatures on overall process efficiency.

Catalyst cracking enables tar elimination at lower temperatures by using a catalytic material to decrease the required activation energy. This method is the most effective for removing tars from producer gas/syngas. Heterogeneous catalysts typically employed for tar elimination can be natural minerals which are generally cheaper than synthetic catalysts. However, rapid catalyst deactivation necessitates specific reactor configurations, such as circulating fluidized bed systems or switch reactors, increasing operational complexity. Additionally, catalyst attrition and irreversible deactivation require substantial catalyst replacement, resulting in higher operational expenditure [6–9]. However, catalyst cracking for tar abatement is beyond the scope of this study.

Partial oxidation (POX) increases the temperature of the syngas by oxidizing a portion of it with oxygen. This process accelerates tar cracking and polymerization pathways different from those observed in pyrolytic thermal decomposition. According to Hoeven et al. [10], oxygen serves as an excellent initiator of free radicals, such as hydrogen (H), oxygen (O), hydroxyl (OH) and hydroperoxy (HO_2), and plays a crucial role in chain initiation and subsequent reactions. Furthermore, oxygen facilitates the exothermic oxidation of hydrocarbons, generating the heat required for propagation reactions. However, an excess amount of oxygen can lead to the production of too many PAHs and even soot [11,12].

Table 1 provides an overview of studies that have examined the potential of thermal cracking and partial oxidation of pyrolysis vapors, model molecules and gasification syngas in reducing tar content. The formation of heavier PAHs from simple aromatics or naphthalene at high temperature has been identified [13,14]. Additionally, soot is produced through a polymerization/sooting mechanism from inlet tars at high

temperature [13,15]. H_2 has been found to act as an inhibitor of PAHs and soot formation [13,16] while steam has a minimal influence on tar reduction [15,16]. High temperature around 1200°C must be reached to achieve 90% tar reduction through thermal cracking [14]. In the partial oxidation, the addition of oxygen can hinder the sooting process and contribute to better tar reduction compared to thermal cracking by promoting the formation of free radicals, thus accelerating tar destruction [12,13,17,18]. The primary tars are transformed into lower molecular weight tars [18].

According to Wu et al., the maximum reduction of tar from pyrolysis vapors at 900°C occurs at an equivalence ratio (ER) of 0.34. However, a higher ER can result in the combustion of non-condensable gases like H_2, CO and CH_4 [12,17]. In the case of a biogasification syngas a tar reduction of 90% can be achieved with an air/fuel ratio of 0.2 [13]. It is worth noting that there are very few studies available that have specifically investigated the partial oxidation of gasifier producer gas, and those that exist have mostly used simulated syngas (refer to Table 1) [13,15].

Table 1: Thermal cracking (TC) and partial oxidation (POX) studies.

Type[a]	Year/author	Experiments *Feedstock/model molecules*	Model	Ref.
Producer gas/syngas				
TC	2004 Houben	Wood (willow) syngas in a TR[b] (L=700 mm, D=75 mm, 0.015-0.6 Nm^3/h	No	[11]
	2009 Valin	Model syngas (CH_4, H_2, CO, CO_2, H_2O, N_2) in a cylindrical reactor (1-2 Nm^3/h)	PFR, two detailed kinetic model compared (127 species, 1207 reactions vs 159 species, 773 reactions)	[19]
POX	2005 Houben	Naphthalene (2.6 mg/Nm^3) in a simulated syngas (H_2, CH_4, N_2) in a combustion burner	No	[13]
	2013 Svensson	Model validation on experimental TC data from [19]	Dynamic model (FDM): 53 species 325 reactions (GRI-Mech 3.0). Static model (series of CSTR): 157 species 872 reactions.	[15]
Model molecules				
TC	1992 Blekkan	CH_4 in a TR[b] (L=1 m, D=9 mm)	No	[20]

	1996 Jess	Naphthalene, toluene and benzene in a TR[b] (L=50 cm, D=20 mm)	10 reactions	[16]
	1999 Sarobe	Acenaphtho[1,2-a]acenaphthylene, Fluoranthene, Benzo[k]- and Benzo[j]fluoranthene in a QT[b] (L=40 cm, D=25 mm)	No	[21]
	2016 Gai	Naphthalene, anthracene in a FB[b] (D=20 mm, H=42 mm)	No	[22]
POX	2007 DeCoster	Anthracene in a two-stage laminar-flow drop-tube furnace	No	[23]
	2008 Thomas	Catechol in a laminar flow QT[b] (D=2 mm)	No	[24]
	2017 Zhang	2-methoxyphenol, anisole, furfural, toluene in a flow QT[b] D=8 mm L=350 mm	Detailed kinetics (201 species, 1100 reactions)	[17]
	2019 Peng	Phenanthrene in a QT[b] D=30 mm L=500 mm	No	[25]
Pyrolysis vapors (PV)				
	2000 Brandt	Wood chips in a two-stage gasifier (100-hWth)	No	[26]
	2001 McGrath	Cellulose and pectin pyrolysis in a two-zone QT[b] (200 mg, 300-600°C)	No	[27]
	2011 Wu	Rice straw in a SP[b] (4 kg/h, 500°C) + electrically heated POX reactor	No	[12]
	2013 Wongchang	Wood in a free fall pyrolyzer (0.536 g/min, 600°C)	No	[14]
	2021 Tanoh	Green waste in a RK[b] (6 kg/h, 800°C) + electrically heated non-catalytic TR[b]	PFR[b] & detailed kinetics	[28]
POX	2011 Su	Rice straw in a SP[b] (1-10 kg/h, 500°C) + electrically heated POX reactor	2D-CFD isothermal 900°C (CO_2, CH_4, H_2, N_2, H_2O, phenol toluene). Tars = benzene, toluene, phenol, naphthalene (16 reactions, 11 species)	[29]
	2011 Wu	See above.		[12]
	2013 Ahrenfeldt	Pine wood in a SP[b] (1.16 kg/h, 600°C) + electrically heated POX reactor	No	[18]
	2014 Weston	Wood pellets in a pyrolyzer (500-800°C, 100 g per batch) + Coanda burner	No	[30]
	2015 Mao	Biomass tar in a micro FB[b] reactor for liquids (H=88 mm).	No	[31]
	2015 Thimthong	Cedar sawdust fast pyrolysis in a tubular vertical TSR[b] (0.09-0.20 g/min, 700-800°C)	PFR[b] & detailed kinetics (8159 reactions, 548 species)	[32]
	2021 Tanoh	See above.		[33]

[a]Thermal cracking (TC) or partial oxidation (POX)

[b]Screw pyrolyzer (SP), plug flow reactor (PFR), two-stage reactor (TSR), fluidized bed (FB) rotary kiln (RK), quartz tube (QT), tubular reactor (TR), diameter (D), length (L).

Significant efforts have been made to develop kinetic mechanisms that provide a deeper understanding of the phenomena involved (as shown in Table 1). These mechanisms are essential for the proper design and scaling up of a POX unit. However, extrapolating the observed mechanisms observed from model molecules and controlled gas environments to a real gasification environment is not a straightforward task due to the complex chemistry of tertiary tars. Given the number of species and the mechanism pathways in such a system, a limited set of reactions is insufficient to accurately replicate the detailed composition at the reactor outlet. Radical kinetic mechanisms have been formulated for thermal cracking and oxidation of biomass products. For instance, Dhahak et al. (2019) developed a comprehensive model of biomass pyrolysis and oxidation that includes PAHs up to chrysene ($C_{18}H_{12}$) as well as a mechanism for NOx formation, encompassing 710 species and 5035 reactions [34]. Norinaga et al. (2009, 2013) developed similar models for thermal cracking under pyrolytic conditions [35,36]. The main advantage of these detailed kinetic models is that they avoid lumping processes. Thus, the detailed composition of the gas is predicted. If computational time is reasonable, such models can enhance the accuracy of process model predictions for tar formation by utilizing complete kinetics and not overly simplified kinetics [37].

In this study, the focus was on investigating the partial oxidation of a real producer gas stream through both experimental and numerical approach. The experimental setup involved conducting partial oxidation experiments in a dedicated partial oxidation unit (POX) that was electrically heated and well-insulated. These experiments were performed downstream of a 5 kg/h air-blown bubbling bed gasification reactor. By utilizing a real syngas instead of a simulated one, the study aimed to achieve greater accuracy since generating the heaviest PAHs in a simulated syngas can be challenging. The results obtained from the POX experiments were compared to reference tests conducted without the POX unit to evaluate the impact of POX reactions on gasification indicators and pollutant contents. To complement the experimental findings, numerical modeling of the POX unit was carried out using ANSYS Chemkin Pro. The composition of the producer gas, which was experimentally measured at the gasification reactor's exit, served as input for the

numerical simulations. The overall objective of this study was to demonstrate the reliability and effectiveness of advanced kinetic modeling techniques when dealing with the complex composition of a real producer gas.

The novelty of this research lies in two key aspects:

1) A comprehensive analysis of the detailed composition of gasification tars before and after partial oxidation in a pilot plant that is coupled with a fluidized bed gasifier. This detailed characterization offers valuable insights into the behavior and transformation of tars during the partial oxidation process.
2) A detailed kinetic model was developed, specifically designed to account for the thermal cracking and oxidation of tars up to C_{24} including soot formation. The model's accuracy and predictive capabilities were validated using a real biomass gasification producer gas.

Overall, this study contributes to advancing the understanding of partial oxidation processes and highlights the importance of employing advanced kinetic modeling approaches when dealing with the complex composition of real producer gases.

2. MATERIAL AND METHODS

2.1. Feedstock, experimental rig and analytical methods

The feedstock material utilized in this study consisted of pellets made from medium density fiber board (MDF). The chemical composition and other properties of the MDF material were thoroughly described in a separate publication [38]. Notably, the nitrogen content in the MDF material was relatively high at 3.5 wt.% (on a dry basis), due to the use of urea-formaldehyde resins for panel fabrication. The water content was approximately 5 wt.%.

The experimental setup for gasification involved the following components: (i) a double-screw feeding system, (ii) an externally heated bubbling bed gasification reactor, where air was used as the gasifying agent, (iii) a cyclone separator and, (iv) a cooling system incorporating a Venturi scrubber.

To analyze the gas composition and tar content, several analytical techniques were employed. The concentration of permanent gases, including N_2, CO, CO_2, H_2, CH_4, C_2H_2, C_2H_6, C_3H_4 and C_3H_6, was measured every 3 minutes using a micro-gas chromatography (μ-GC) with N_2 as the tracer gas. Tar molecules were collected in a series of wet impingers filled with 2-propanol and quantified by GC-MS-FID and HPLC-UV. Additionally, a semi-quantitative analysis of light and heavy tar molecules was conducted using Synchronous Fluorescence Spectroscopy (SFS). SFS is a rapid technique that utilizes the correlation between the emission spectral band and the number of aromatic rings, particularly for linear PAHs [39]. A comprehensive description of the experimental setup and all analytical methods can be found in the referenced publication [38].

2.1.1. Partial oxidation unit

A scheme of the oxidation unit (POX) developed at LRGP is depicted in Figure 1. The POX unit was coupled downstream of the cyclone separator and consisted of several components: a pre-heating chamber, a non-premixed swirl coaxial burner, a reaction chamber and a cooling zone.

The producer gas stream, coming from the cyclone, entered the preheating chamber of the POX unit at approximately atmospheric pressure. From there, the gas stream passed through the central tube of the burner and was mixed with an airflow injected tangentially by the swirl coaxial burner. The gas-centered swirl coaxial burner comprised a pre-injection chamber where the airflow was equally distributed to five injection holes, each with a diameter of 3.5 mm. These injection holes were inclined at a 45° angle with respect to the two axes, creating a turbulent flow to ensure efficient mixing of the gases. The secondary air flow was injected at constant flow rate, controlled by a mass flow controller (Brooks 5851s). In some tests, the air was preheated before entering the POX unit. During preliminary design simulations, it was observed that local high-temperature spots (~2000 K) developed in the zone adjacent to the injection. To prevent damage to the reactor walls, which were made of SIRIUS steel, the reaction chamber was enclosed by an inner tube of SiC with a thickness of 1 cm. The space between the inner SiC tube and the outer SIRIUS steel was left empty to minimize heat transfer by conduction. The reaction chamber's final volume, located inside the SiC tube, was approximatively 11.5 L (inner diameter 10.2 cm, length 140 cm). To maintain a uniform temperature, the POX unit was uniformly heated by an external oven, which helped compensate for heat losses resulting from the small size of the pilot plant. Finally, a cooling chamber was positioned at the bottom of the POX unit.

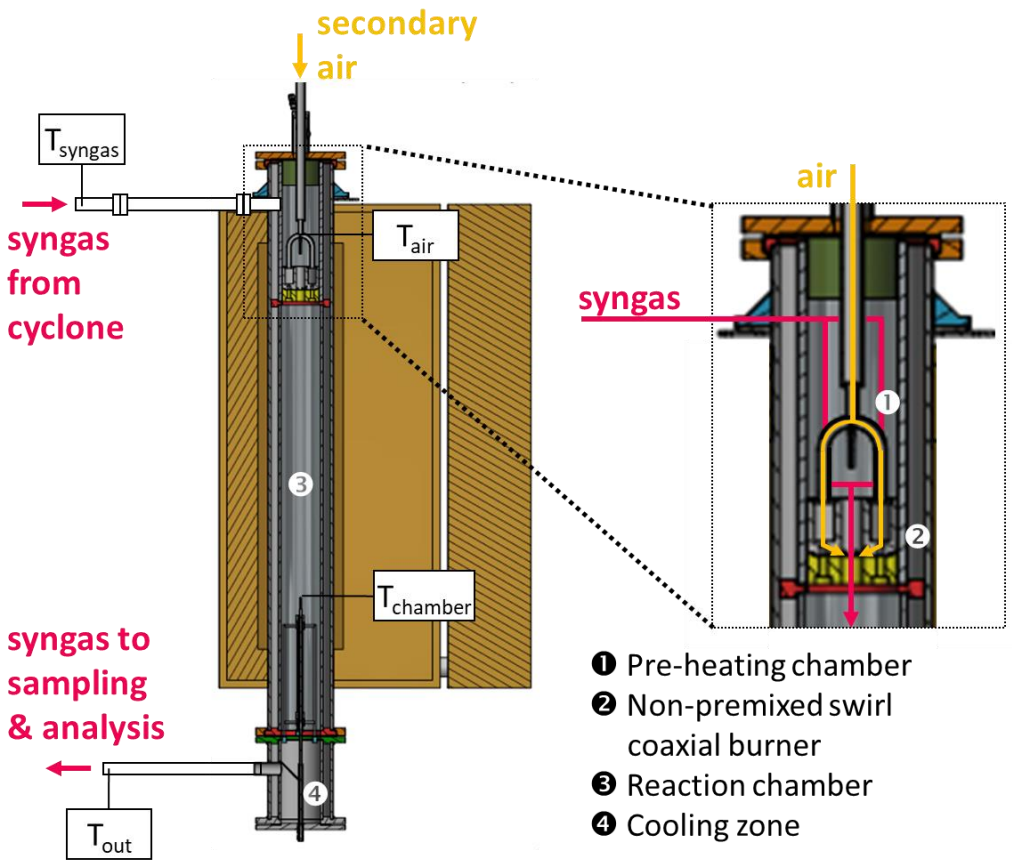

Figure 1: Scheme of the POX unit.

Temperature measurements were taken at crucial points within the POX unit (see Figure 1) and corresponds to: the inlet of the producer gas to the swirl burner (T_{syngas}), the inlet of airflow to the pre-distribution chamber (T_{air}), the temperature of the reaction chamber ($T_{chamber}$) and the temperature at the exit of the cooling zone (T_{out}). The thermocouple of the reaction chamber was centered by a radial support and placed at the end of the reaction chamber. The temperature of this thermocouple was used to monitor the reaction chamber.

2.1.2. Experimental conditions

In order to evaluate the impact of POX reactions on gasification, the results obtained for the POX tests were compared with three repeated reference tests (REF) that were conducted without the POX unit and

described elsewhere [38]. The main operating parameters of the gasification reactor, including the reactor temperature, feedstock flow rate, primary air flowrate and test duration, were maintained constant for all tests. These parameters were set to 800°C, 4.4 kg/h, 4.5 Nm^3/h and 2 h, respectively. The air-to-fuel equivalence ratio (ER) inside the reactor was also kept constant at 0.25 for all tests. Previous publications have explored the variations of these parameters and their influence on syngas production [38,40]. A total of 4 POX tests were conducted, specifically varying the temperature and secondary air flow rate. Table 2 provide a summary of the targeted values for the different parameters in these four POX tests.

Table 2: Operating parameters of the partial oxidation unit.

Test (ER-$T_{chamber}$)	**REF**	**0.05-1025**	**0.1-1034**	**0.1-1059**	**0.1-1100**
Secondary air flow rate (NL/h)	-	1000	2000	2000	2000
Temperature set-point of secondary air preheating, °C	-	20	20	500	500
Temperature set-point of the POX unit external oven, °C	-	1100	1100	1150	1200
ER secondary	-	0.05	0.1	0.1	0.1
ER total	0.25	0.30	0.35	0.35	0.35

2.2. Modeling and numerical methods

2.2.1. Kinetic mechanism

A detailed radical kinetic mechanism was developed to describe the oxidation and formation of biomass tars. The mechanism was constructed by merging two main mechanisms obtained from various literature sources [34–36,41]. The first component of the mechanism, BioPOX-2 was originally developed by Darido et al. [42], which was an extension of BioPOX-1 from Dhahak et al. [34] (634 species and 4759 reactions). BioPOX-2 includes the kinetics of biomass pyrolysis and oxidation, as well as the formation of PAHs up to chrysene ($C_{18}H_{12}$). It also incorporates a mechanism for NOx formation.

The second component of the mechanism was derived from the work of Norinaga et al. (2009) [35], which focused on pyrolysis conditions. This mechanism was used to include the kinetics of heavy PAHs ranging from C_{10} to C_{24} which were measured in the experiments but not accounted for in the BioPOX-2 mechanism. Furthermore, additional oxidation reactions for these heavy PAHs were incorporated from the work of Norinaga et al. (2013) [36]. To account for the oxidation of fluorene, which is an important reaction product, an extra lumped reaction (1) was included in the mechanism. The formulation of this reaction followed the methodology employed by the CRECK modeling group of Politecnico di Milano [43], and the kinetic parameters recommended by this group [44].

$$fluorene + OH \rightarrow H + CO + biphenyl \quad (1)$$

Phenanthrene and anthracene, which were originally lumped together in the BioPOX-2 mechanism, were treated as separate species. These two species were measured separately in experiments and follow different reactions paths in Norinaga's mechanisms.

Regarding the formation of soot, it is generally accepted that soot is a product of partial oxidation reactions. In line with previous findings by Saggese et al. [45], it was assumed that soot originates from C_{20} precursors. Therefore, reactions 2 and 3 were included in the mechanism to provide an estimate of soot formation and growth from acetylene [41]. The kinetic parameters for these reactions can be found in Table 3.

$$C_{\mathrm{n}}H_{\mathrm{m}} \rightarrow \mathrm{n}C_{soot} + \frac{\mathrm{m}}{2}H_2 \quad (2)$$

$$C_2H_2 + C_{soot} \rightarrow 3C_{soot} + H_2 \quad (3)$$

Table 3: Kinetic parameters.

Reaction	A	Ea (cal/mol)	Ref
1	$4.0 \cdot 10^{13}$ s^{-1}	$7.0 \cdot 10^{3}$	[44]
2	$5.0 \cdot 10^{6}$ s^{-1}	$3.99 \cdot 10^{4}$	[41]
3	$2.5 \cdot 10^{8}$ $cm^{3}mol^{-1}s^{-1}$	$9.99 \cdot 10^{3}$	[41]

The SYNPOX model for SYNgas Partial OXidation - contained 742 species and 5093 reactions. This kinetic model can be found in the Supplementary material.

To validate the SYNPOX model, experimental data from Tanoh's study [36], were utilized. This comparison includes a wide range of species including light gases such as H_2, CH_4, CO, CO_2, acetylene, ethylene, and water, as well as eight aromatics and PAHs from benzene up to pyrene. It also includes comparisons with tar, gas and soot mass fractions. The overall agreement is quite satisfactory for all species and for thermal cracking and steam cracking conditions (see section 8.2 in Supplementary Material).

2.2.2. Plug-flow reactor model

The POX pilot was simulated using an ideal plug-flow reactor model with dimensons matching the reaction chamber of the POX unit (10.2 cm in diameter and 1.1 m in length). The simulation was performed using ANSYS Chemkin Pro 17.0 and a Python software interface was utilized for easier management of the results. The inlet composition of the syngas was obtained from the REF experiments (gasification test without POX unit). The syngas and air were assumed to be premixed and injected at the inlet of the reactor. The inlet temperature was calculated using the RK-ASPEN thermodynamic model in AspenPlus 8.8. The pressure was assumed to be constant and close to atmospheric, while the air composition was considered to be 21%v O_2 and 79%v N_2. The 1D-model assumed that the gas temperature was radially uniform and equal to the temperature measured by the thermocouple ($T_{chamber}$ temperature).

In an industrial-scale POX unit, the thermal conditions would typically approach adiabatic conditions. However, due to the scale of the pilot plant, it was necessary to heat the reactor to compensate for heat losses at the reactor's surface. The heat transfer mechanism in this setup is complex, involving convection

and conduction heat transfer through the layers of the reactor (including the inox outer layer and the annular gap between the outer layer and the SiC inner layer). Radiative heat fluxes between the oven and the reactor's outer layer, as well as between the metal layers and the inner surface, also need to be determined. Additionally, the presence of soot in the gas phase further complicates the heat transfer analysis. The heat flux profile from the oven is likely not uniform along the POX chamber in the experimental setup. Considering these complexities and uncertainties, it is more appropriate at this stage to use an isothermal condition based on a real measurement, rather than making assumptions about the heat flux using a specific boundary condition such as $q = U \cdot (T_{gas} - T_{surface})$ or $q = q_0$.

Table 4: Boundary conditions of the CHEMKIN PRO plug flow model

Reactor model	Test	T inlet (°C)	T chamber measured (°C)	Inlet volumetric flowrate (standard m^3/min at 298.15K)
Ideal plug flow	0.05-1025	599	1025	0.188
	0.10-1034	555	1034	0.206
	0.10-1059	607	1059	0.206
	0.10-1100	674	1100	0.206

3. RESULTS AND DISCUSSION

3.1. Partial oxidation cracking tests

Table 5 details the main temperatures, gas composition and product yields for both reference (REF) and POX tests. The tar yields as shown in Figure **2**, were classified according to the ECN tar classification system [46]: class 2 for heterocyclic components, class 3 for light hydrocarbons without condensation and water solubility issues, class 4 for 2-3 rings PAHs and class 5 for heavy polyaromatic hydrocarbons (4-5 rings PAH's). The yields of all gas and tar molecules quantified in this study were detailed in Table S1 (supplementary materials).

From Table 5, it can be observed that the temperature achieved inside the POX unit were close to the targeted temperatures. In all POX tests, the temperature inside the reaction chamber exhibited a slight increase during the first 30 minutes of the test and then remained steady. The lower temperatures measured at the inlet of the secondary air stream for the tests 0.05-1025 and 0.1-1034 were a result of the absence of air preheating in these cases.

Comparing to the average gas concentrations between the reference test (REF) and the four POX tests, a clear decrease in CH_4, C_2-C_3 hydrocarbons and benzene can be observed, while there is a marked increase in CO and acetylene (C_2H_2). This decrease in light hydrocarbons and benzene leads to a decrease in the volumetric LHV of the gas. The introduction of additional air flow in the tests 0.05-1025 and 0.1-1034 resulted in an increase in H_2 and CO concentrations, and a decrease in CO_2 and C_2H_2. The increase in the temperature of the reaction chamber in the tests 0.1-1034, 0.1-1059 and 0.1-1100 did not show any notable global trend, within experimental uncertainty. However, the methane concentration decreases with the temperature increase in the tests with an ER of 0.10, which is consistent with thermal cracking of methane above 1000°C, as observed by Valin et al. [47].

The residual concentration of O_2 in the syngas analyzed could result from imperfect syngas and air mixing in the POX or from air linkage during sampling and analysis.

The test 0.1-1034 exhibits noticeable higher cold gas efficiency, carbon and hydrogen conversions. However, this may be attributed to an overestimate of the gas yield in this particular test.

Table 5: Main operation conditions, gasification indicators and products yield in reference and partial oxidation experiments.

Case	REF	0.05-1025	0.1-1034	0.1-1059	0.1-1100
Gasifier					
Test duration, h		1.43	1.73	1.61	1.38
Consumed feed, kg (as received)		6.6	7.96	8.04	6.3
Fuel feed rate, kg/h	4.5 ± 0.1	4.6	4.6	4.5	4.6
Bed temperature, °C	800 ± 2	794	789	801	796
Freeboard temperature, °C	757 ± 1	761	762	765	762
ER (reactor)	0.25 ± 0.01	0.25	0.25	0.25	0.25
Partial oxidation unit					
Secondary air flow rate, NL/h	-	1020	1980	1980	1980
Air preheating set-point, °C	-	-	-	500	500
Airflow inlet T_{air}, °C	-	406[b]	304[b]	466	565
Producer gas inlet T_{syngas}, °C	-	614	587	629	691
POX external oven set-point, °C	-	1100	1100	1150	1200
Reaction chamber $T_{chamber}$, °C	-	1025	1034	1059	1100
Cooling chamber exit T_{out}, °C	-	647	601	657	668
Gas residence time, s	-	1.0	0.9	0.9	0.9
ER (total)	0.25 ± 0.01	0.30	0.36	0.37	0.36
Syngas indicators					
Gas Yield η_{syngas}, Nm^3/kg feed (daf)	1.78 ± 0.05	2.03	2.33	2.27	2.24
LHV_{syngas}, MJ/Nm^3	4.54± 0.05	3.82	4.16	3.63	3.43
Cold gas efficiency %CGE[c]	44.3 ± 0.02	42.5	53.4	45.2	42.8
Carbon conversion %C[d]	76.8 ± 0.02	64.2	76.1	72.0	67.0
Hydrogen conversion %H[d]	48.0 ± 0.02	42.9	52.6	44.4	42.6
Gas composition, $\%_{mol}$ (N_2 free, dry)					
H_2	17.4 ± 0.6	16.4	18.3	18.0	19.9
CO	29.3 ± 0.2	31.9	36.7	35.5	34.5
CO_2	39.8 ± 0.4	38.1	32.5	36.7	35.8
CH_4	9.1 ± 0.1	8.7	8.5	7.0	6.1
C_2H_2	0.33 ± 0.02	1.54	1.33	1.35	1.26
C_2H_4	3.0 ± 0.1	1.0	0.4	0.3	0.2
C_2H_6	0.36 ± 0.01	0.01	0	0	0
C_3H_4	0.04 ± 0.004	0.02	0.02	0.01	0.01
C_3H_6	0.29 ± 0.04	0.01	0.01	0	0

O_2	0.4 ± 0.2	2.3	2.3	1.1	2.4
Tar yield, g/kg$_{feed}$ (daf)					
Total[a]	11.6 ± 0.2	4.7	1.7	2.0	1.4
Gas dew point, °C	171.7	188.1	184.0	183.7	187.5
Water and acid gas yields, g/kg$_{feed}$ (daf)					
NH_3	18.5 ± 4.9	19.2	25.9	27.8	18.9
HCN	2.5 ± 0.3	3.2	1.4	6.2	6.0
H_2O	342 ± 13	386	361	388	389

[a]Total tar yield was calculated excluding benzene.

[b]No preheating for secondary air.

[c]$\%CGE = \frac{LHV_{syngas}}{LHV_{feed}} \cdot \eta_{syngas}$

[d]$\%C = \frac{\dot{m}_{C,gas}}{\dot{m}_{C,biomass}}$; $\%H = \frac{\dot{m}_{H,gas}}{\dot{m}_{H,biomass}}$ where $\dot{m}_{C,gas}$ and $\dot{m}_{H,gas}$ are the carbon and hydrogen mass flowrates in the gas generated (permanent gases: H_2, CO, CO_2, CH_4, C_2H_2, C_2H_4, C_2H_6, C_3H_4, C_3H_6), $\dot{m}_{C,biomass}$ and $\dot{m}_{C,biomass}$ the carbon and hydrogen mass flowrates from the biomass.

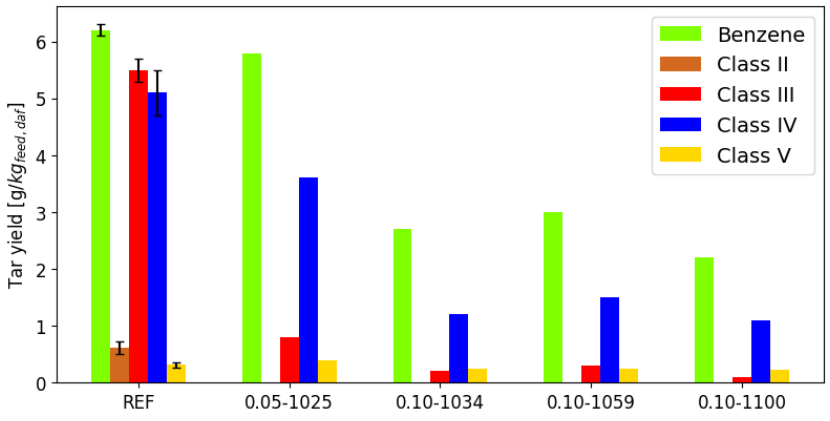

Figure 2: Tar composition in the different tests (tar groups according the ECN tar classification).

Compared to the REF test, the POX tests conducted with a secondary ER of 0.05 and 0.1 resulted in a significant reduction in overall tar yield, by 60% and 90%, respectively. In terms of tar concentration, the POX unit led to a decrease from 6.5 g/Nm^3 (dry gas, C_6H_6-free) in the REF tests to 2.3 g/Nm^3 (dry gas, C_6H_6-free) in the test 0.05-1025. Furthermore, increasing the secondary air flow in the test 0.1-1034 further reduced the tar concentration to 0.72 g/Nm^3 (dry gas, C_6H_6-free). On the other hand, the increase in the temperature of the reaction chamber did not show any significant variation in the overall tar yield within experimental uncertainty. This finding confirms that the main factor in tar reduction is the addition of external oxygen. Inside the POX unit, the chemical composition of tars underwent substantially

289 modifications. For example, in the test 0.05-1025 compared to the REF values, there was a drastic
290 reduction in the yields of tar groups II, III and IV by 100%, 86% and 30%, respectively. On the other hand,
291 the yield of group V increased by 26%. A closer examination of individual tar yields, detailed in Table S1
292 (supplementary materials), revealed a significant increase in certain molecules of group IV, such as
293 phenanthrene and fluoranthene, as well as other heavier molecules from group V present in trace
294 concentrations, such as benzo[b]fluoranthene, benzo[a]pyrene, dibenzo[a,h]anthracene,
295 benzo[ghi]perylene and indeno[1,2,3-cd]pyrene. Conversely, there was a reduction in the yields of some
296 molecules of group IV, including naphthalene, acenaphthylene, fluorene and anthracene, which explains
297 the 30% overall drop observed for the group. This observation aligns with previous studies as the
298 production of heavier tars from naphthalene observed by Houben et al. [13]. Moreover, increasing the
299 secondary air flow rate in the test 0.1-1034 led to a more severe reduction in the yields of groups IV and
300 V. In this case, all molecules of group IV showed a negative yield. These results suggest a dependence on
301 the amount of oxygen available through secondary air injection, indicating the influence of secondary air
302 on the unit's efficiency, as observed in previous studies [12,18,26,29]. The tar reduction also resulted in
303 the consumption of light hydrocarbons and benzene, which can be beneficial for further upgrading of the
304 syngas to produce H_2 or CH_4.

305 The substantial modifications in the chemical composition of tars caused by the POX reactions were further
306 supported by synchronous fluorescence spectra (SFS). Figure 3 displays the SFS of tar samples
307 corresponding to reference and POX tests. These results clearly indicate a decrease in the tar content in
308 the producer gas and a shift to longer wavelengths, indicating a predominance of heavy tars in the overall
309 composition.

310 Finally, the yield of water increased after the POX tests due to oxidation reactions. The water composition
311 was calculated by difference based on the overall atomic mass balance. The ammonia composition remains

approximatively constant within the uncertainty range, around ± 4.9 g/$kg_{feed\ daf}$, as observed through repeated REF tests. No clear trend was observed when varying temperature or ER. A slight increase in HCN was observed, reaching approximately twice the inlet feed rate at the highest temperatures. The global nitrogen content in the syngas slightly increased with temperature.

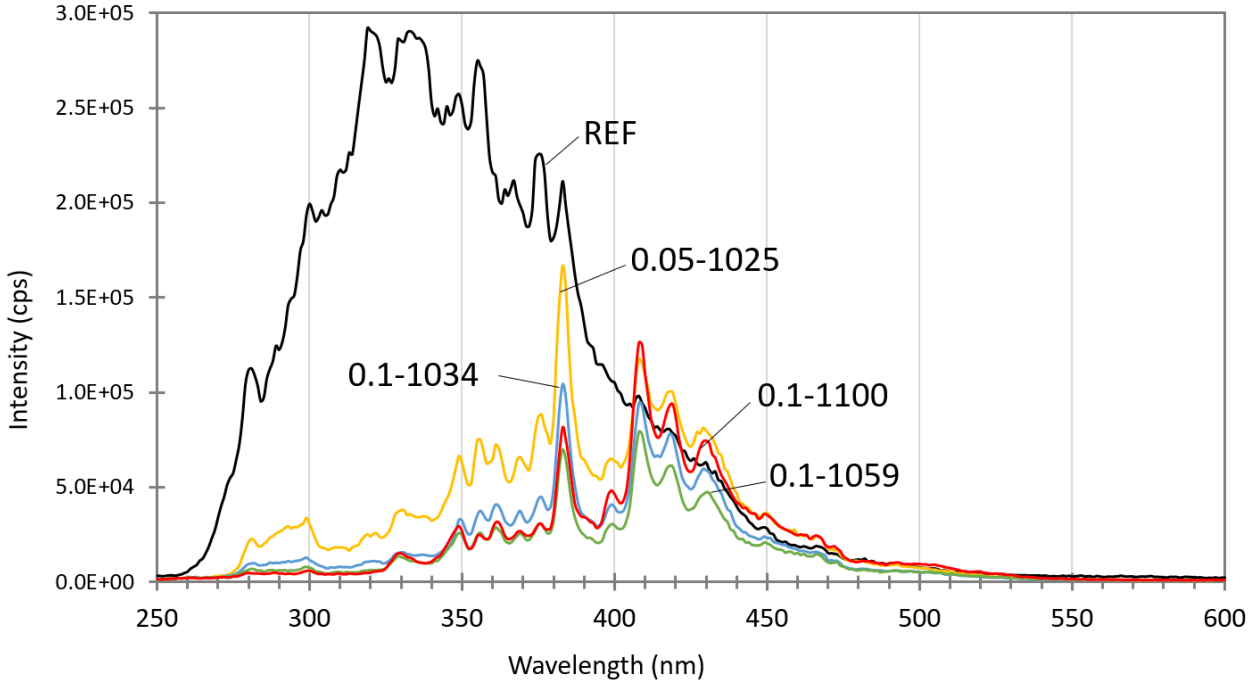

Figure 3: Synchronous Fluorescence spectra (offset = 20 nm).

3.2. Modeling results

In the subsection, two specific cases are presented for conciseness. The two tests with the most different conditions are chosen. Tests 0.05-1025 and 0.10-1100 present two different ER, with and without air preheating. The detailed analysis of the other two cases can be found in Supplementary Material 3.

The detailed composition of the syngas at the inlet and outlet is shown in Figure 4 for ER = 0.5 and Figure 5 ER = 0.10. These figures also include a comparison with the model results. The results demonstrate a good agreement between the experimental data and the plug flow model for the permanent gases (H_2, CO, CO_2, CH_4). The fate of lights hydrocarbons was accurately reproduced, showing an increase in acetylene and a decrease in others C_2-C_3 hydrocarbons.

The model successfully reproduced the trends observed in the tar composition regrouped by ECN classes. Tar classes II to IV decreased, while class V increased at lower ER (0.05-1025) and showed slight reductions or remained stable at higher ER (0.10-1100). Overall, the model's predictions aligned with experimental observations, particularly at the higher ER (0.10). However, there were discrepancies for certain individual tar species such as phenylethyne, acenaphthene and heavy PAHs (C_{20+}), where the model did not accurately predict their behavior. This discrepancy could be attributed to the chosen mechanism for soot formation, which considers C_{20+} as precursors. Additionally, the prediction of tar class V was reasonably satisfactory in case of ER = 0.10 (experimental reduction of 24% compared to a model reduction of 22%). This can be attributed to the predominance of pyrene in class V tars, while other heavy PAH components were present in trace amounts in the experiments (Figures S3 and S4 in supplementary material). The model is able to give global trends in case 0.05-1025 but is not necessarily optimized for all individual species. It should be noted that the isothermal profile assumed in the plug flow model may differ significantly from the actual thermal profile in the experimental setup. For the acid gases the prediction for NH_3 fell within the uncertainty range, but HCN consumption contradicted the experimental increase observed in case of 0.10-1100.

Regarding soot formation, the model predicts an increase with temperature (Table 6). Although soot collection was not performed in the present work, the excellent agreement between the computed data using the SYNPOX model and literature experimental data obtained by [33] under similar thermal cracking

and oxidative conditions around 1200°C (slightly higher than the present study) suggests that the predicted trend for soot formation under the present study conditions is likely valid. The validation comparison sets of the SYNPOX model are presented in Supplementary Material 2. This tend to confirm that heavy PAHs C_{20+} are soot precursors [45].

Table 6: Soot production and tar reduction.

Case (ER-$T_{chamber}$)	**0.05-1025**		**0.10-1034**		**0.10-1059**		**0.10-1100**	
	Exp.	Model	Exp.	Model	Exp.	Model	Exp.	Model
Soot production ($mg/kg_{biomass\ dry}$)		49.1		45.0		62.2		102.3
Tars class II	-100%	-90%	-100%	-97%	-100%	-98%	-100%	-99%
Tars class III	-81%	-86%	-96%	-95%	-95%	-95%	-98%	-95%
Tars class IV	-30%	-46%	-76%	-69%	-71%	-70%	-78%	-72%
Tars class V	+23%	+49%	-27%	-1%	-26%	-7%	-24%	-22%

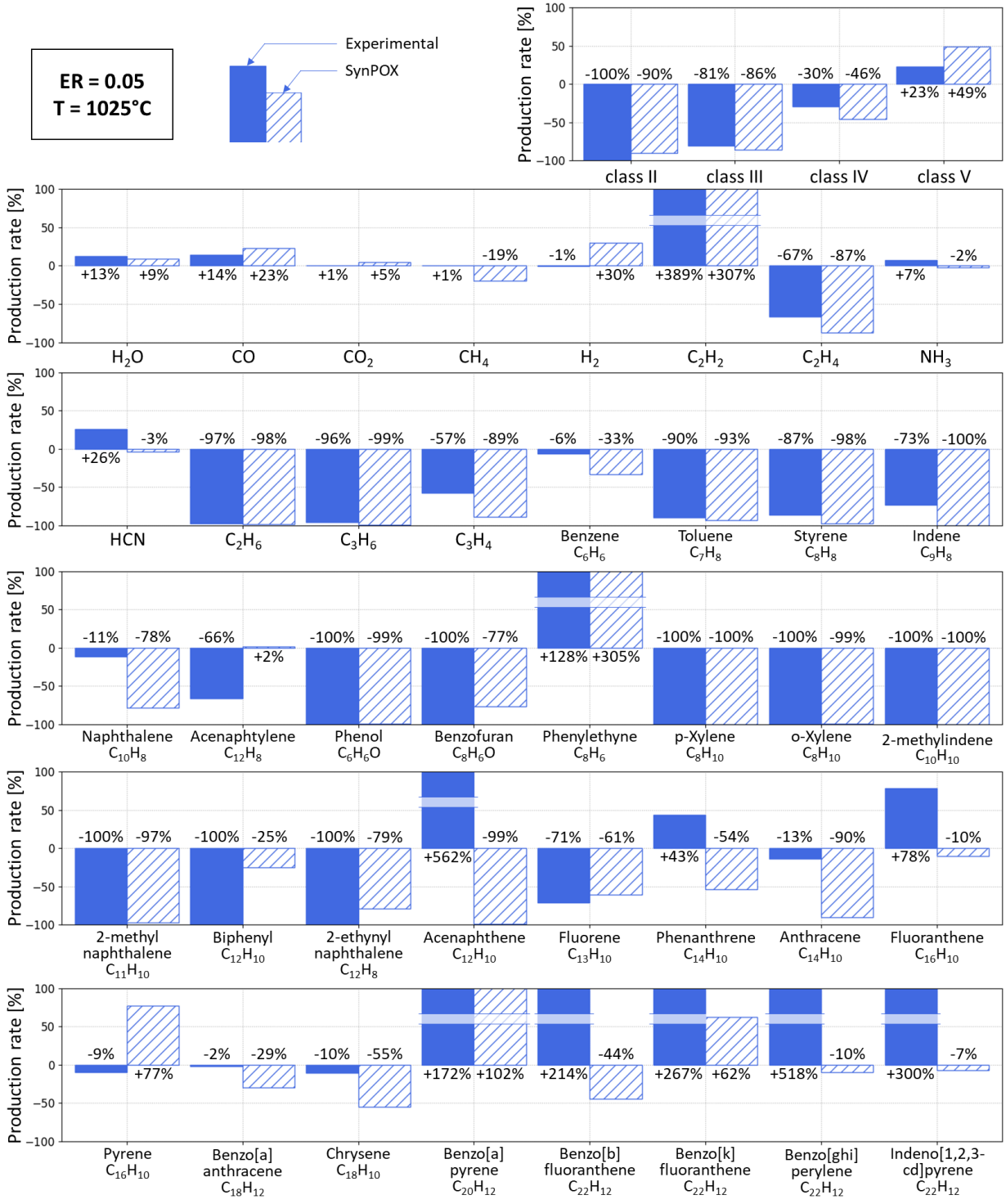

353

354 **Figure 4: Experimental and modelled syngas production rate after POX unit for case 0.05-1025.**

355 **Simulated composition from plug flow.**

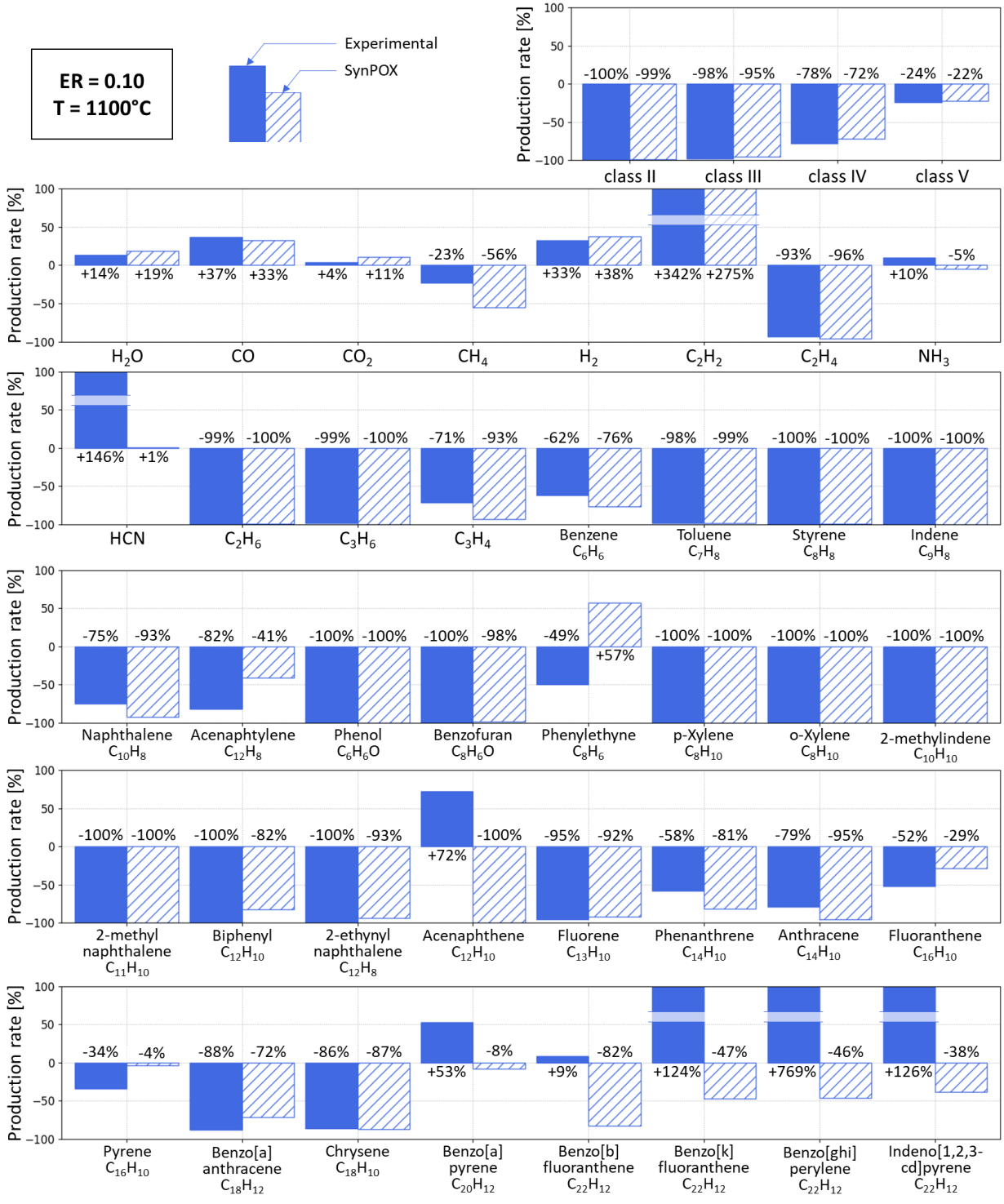

Figure 5: Experimental and modelled syngas production rate after POX unit for case 0.10-1100. Simulated composition from plug flow.

Based on the results obtained, the following recommendations can be made:

- To significantly reduce the tar content, an equivalence ratio around 0.10 must be reached.
- An attention should be made on the production of heavy PAHs and the formation of soot.
- The partial oxidation unit could contribute to the enrichment of syngas in CO and H_2.

This kinetic mechanism developed in this study provides a valuable tool for estimating the potential reduction of tars through partial oxidation, considering parameters such as residence time and amount of oxygen. Despite the complexity of the kinetic model (hundreds of species including radicals and thousands of reactions), the 1D plug flow model offers a fast and efficient solution. This model can be coupled with process modeling software, such as Aspen Plus, to incorporate realistic complex systems beyond the scope of model molecules [48].

It is worth noting that the assumption of perfect mixing at the inlet of the plug flow reactor may be questionable, particularly due to the presence of high oxygen concentration zones near the air nozzles, which can lead to localized hot spots. To gain deeper insights into these hot spots and improve the prediction of heavy PAHs, the kinetic model could be incorporated into computational fluid dynamics (CFD) simulations. This type of simulation would provide more accurate predictions for heavy PAHs and contribute to the design and optimization of partial oxidation units.

4. CONCLUSION

This study presented detailed composition of syngas produced from a biomass gasification fluidized bed reactor (5 kg/h pilot-scale) coupled with a partial oxidation unit. The secondary air injected to the POX unit was varied with different equivalence ratio (0.05 and 0.10) and with or without air preheating to examine the impact of temperature on the unit efficiency. The results demonstrated a significant reduction in tar

content ranging from 59 to 88% under these conditions. The addition of oxygen was found to be the primary factor contributing to this reduction, rather than temperature increase. To achieve a 90% reduction in tars, an equivalence ratio of 0.10 was recommended.

The reduction in tars was accompanied by an increase in the average molecular weight of PAHs, which are known precursors for soot formation. The partial oxidation also led to an enrichment of CO and H_2 concentrations in the syngas.

Additionally, a detailed radical kinetic model was developed and refined to incorporate the formation of heavier tars and soot. The model results were compared to experimental data and showed a good overall agreement, particularly for the equivalence ratio of 0.10. The major components and most tar molecules were accurately modeled.

These data and kinetic model offer the opportunity to simulate and optimize partial oxidation units without compromising the complexity of the involved species and kinetic mechanisms. By integrating the kinetic model into computational fluid dynamics (CFD) models, a more comprehensive understanding of the complex hydrodynamics and critical design aspects of such units can be achieved.

5. SUPPORTING INFORMATIONS

The supporting information files 1 and 2 presents the thermodynamic properties of SynPOX model and the kinetic model. The supporting information file 3 presents: 1) the detailed product composition of each experiment, 2) a validation of the SynPOX model for the soot formation, and 3) additional results for the cases not presented in the full-length article (0.1-1034 and 0.1-1059).

6. FUNDINGS

This work was funded by the French PIA project “Lorraine Université d’Excellence” (reference ANR-15-IDEX-04-LUE), by the COMETE project (FEDER European fundings) and by the Labcom ASTARTE (ANR 15-LCV4-0004-01).

7. REFERENCES

[1] Smil V. Energy Transitions: Global and National Perspectives. Second edition. Santa Barbara, California Denver, Colorado: Praeger, an imprint of ABC-CLIO, LLC; 2017.
[2] Woolcock PJ, Brown RC. A review of cleaning technologies for biomass-derived syngas. Biomass and Bioenergy 2013;52:54–84. https://doi.org/10.1016/j.biombioe.2013.02.036.
[3] Jenbacher GE. Technical Instruction No.: 1000-0302. Fuel Gas Quality, Special Gases 2009.
[4] Bensabath T, Monnier H, Glaude P-A. Detailed kinetic modeling of the formation of toxic polycyclic aromatic hydrocarbons (PAHs) coming from pyrolysis in low-pressure gas carburizing conditions. Journal of Analytical and Applied Pyrolysis 2016;122:342–54. https://doi.org/10.1016/j.jaap.2016.09.007.
[5] Yu J, Guo Q, Gong Y, Ding L, Wang J, Yu G. A review of the effects of alkali and alkaline earth metal species on biomass gasification. Fuel Processing Technology 2021;214:106723. https://doi.org/10.1016/j.fuproc.2021.106723.
[6] Valderrama Rios ML, González AM, Lora EES, Almazán del Olmo OA. Reduction of tar generated during biomass gasification: A review. Biomass and Bioenergy 2018;108:345–70. https://doi.org/10.1016/j.biombioe.2017.12.002.
[7] Ren J, Cao J-P, Zhao X-Y, Yang F-L, Wei X-Y. Recent advances in syngas production from biomass catalytic gasification: A critical review on reactors, catalysts, catalytic mechanisms and mathematical models. Renewable and Sustainable Energy Reviews 2019;116:109426. https://doi.org/10.1016/j.rser.2019.109426.
[8] Anis S, Zainal ZA. Tar reduction in biomass producer gas via mechanical, catalytic and thermal methods: A review. Renewable and Sustainable Energy Reviews 2011;15:2355–77. https://doi.org/10.1016/j.rser.2011.02.018.
[9] Shen Y, Yoshikawa K. Recent progresses in catalytic tar elimination during biomass gasification or pyrolysis—A review. Renewable and Sustainable Energy Reviews 2013;21:371–92. https://doi.org/10.1016/j.rser.2012.12.062.
[10] van der Hoeven TA. Partial product gas combustion for tar reduction. Dissertation Abstracts International 2007;68. https://doi.org/10.6100/IR616553.
[11] Houben MP. Analysis of tar removal in a partial oxidation burner 2004. https://doi.org/10.6100/IR572600.
[12] Wu W, Luo Y, Chen Y, Su Y, Zhang Y, Zhao S, et al. Experimental Investigation of Tar Conversion under Inert and Partial Oxidation Conditions in a Continuous Reactor. Energy Fuels 2011;25:2721–9. https://doi.org/10.1021/ef200297s.
[13] Houben M, Delange H, Vansteenhoven A. Tar reduction through partial combustion of fuel gas. Fuel 2005;84:817–24. https://doi.org/10.1016/j.fuel.2004.12.013.

[14] Wongchang T, Patumsawad S, Fungtammasan B. An Analysis of Wood Pyrolysis Tar from High Temperature Thermal Cracking Process. Energy Sources, Part A: Recovery, Utilization, and Environmental Effects 2013;35:926–35. https://doi.org/10.1080/15567036.2012.707748.
[15] Svensson H, Tunå P, Hulteberg C, Brandin J. Modeling of soot formation during partial oxidation of producer gas. Fuel 2013;106:271–8. https://doi.org/10.1016/j.fuel.2012.10.061.
[16] Jess A. Mechanisms and kinetics of thermal reactions of aromatic hydrocarbons from pyrolysis of solid fuels. Fuel 1996;75:1441–8. https://doi.org/10.1016/0016-2361(96)00136-6.
[17] Zhang R, Zhao S, Luo Y. Experimental and Modeling Investigation on the Effect of Intrinsic and Extrinsic Oxygen on Biomass Tar Decomposition. Energy Fuels 2017;31:8665–73. https://doi.org/10.1021/acs.energyfuels.7b00989.
[18] Ahrenfeldt J, Egsgaard H, Stelte W, Thomsen T, Henriksen UB. The influence of partial oxidation mechanisms on tar destruction in TwoStage biomass gasification. Fuel 2013;112:662–80. https://doi.org/10.1016/j.fuel.2012.09.048.
[19] Valin S, Cances J, Castelli P, Thiery S, Dufour A, Boissonnet G, et al. Upgrading biomass pyrolysis gas by conversion of methane at high temperature: Experiments and modelling. Fuel 2009;88:834–42. https://doi.org/10.1016/j.fuel.2008.11.033.
[20] Blekkan EA, Myrstad R, Olsvik O, Rokstad OA. Characterization of tars and coke formed during the pyrolysis of methane in a tubular reactor. Carbon 1992;30:665–73. https://doi.org/10.1016/0008-6223(92)90186-Z.
[21] Sarobe M, Kwint HC, Fleer T, Havenith RWA, Jenneskens LW, Vlietstra EJ, et al. Flash Vacuum Thermolysis of Acenaphtho[1,2-a]acenaphthylene, Fluoranthene, Benzo[k]- and Benzo[j]fluoranthene – Homolytic Scission of Carbon-Carbon Single Bonds of Internally Fused Cyclopenta Moieties at T ≥ 1100 °C. Eur J Org Chem 1999;5:1191–200. https://doi.org/10.1002/(SICI)1099-0690(199905)1999:5%3C1191::AID-EJOC1191%3E3.0.CO;2-W.
[22] Gai C, Dong Y, Yang S, Zhang Z, Liang J, Li J. Thermal decomposition kinetics of light polycyclic aromatic hydrocarbons as surrogate biomass tar. RSC Adv 2016;6:83154–62. https://doi.org/10.1039/C6RA15513H.
[23] DeCoster J, Ergut A, Levendis YA, Richter H, Howard JB, Carlson JB. PAH emissions from high-temperature oxidation of vaporized anthracene. Proceedings of the Combustion Institute 2007;31:491–9. https://doi.org/10.1016/j.proci.2006.07.211.
[24] Thomas S, Wornat MJ. The effects of oxygen on the yields of polycyclic aromatic hydrocarbons formed during the pyrolysis and fuel-rich oxidation of catechol. Fuel 2008;87:768–81. https://doi.org/10.1016/j.fuel.2007.07.016.
[25] Peng N, Huang C, Su J. An experimental and kinetic study of thermal decomposition of phenanthrene. Journal of Hazardous Materials 2019;365:565–71. https://doi.org/10.1016/j.jhazmat.2018.11.026.
[26] Brandt P, Larsen E, Henriksen U. High Tar Reduction in a Two-Stage Gasifier. Energy Fuels 2000;14:816–9. https://doi.org/10.1021/ef990182m.
[27] McGrath T, Sharma R, Hajaligol M. An experimental investigation into the formation of polycyclic-aromatic hydrocarbons (PAH) from pyrolysis of biomass materials. Fuel 2001;80:1787–97. https://doi.org/10.1016/S0016-2361(01)00062-X.
[28] Tanoh TS, Ait Oumeziane A, Lemonon J, Escudero-Sanz FJ, Salvador S. A novel two-stage gasification strategy for nitrogen-free syngas production- pilot-scale experiments. Fuel Processing Technology 2021;217:106821. https://doi.org/10.1016/j.fuproc.2021.106821.
[29] Su Y, Luo Y, Chen Y, Wu W, Zhang Y. Experimental and numerical investigation of tar destruction under partial oxidation environment. Fuel Processing Technology 2011;92:1513–24. https://doi.org/10.1016/j.fuproc.2011.03.013.

[30] Weston PM, Sharifi V, Swithenbank J. Destruction of Tar in a Novel Coandă Tar Cracking System. Energy Fuels 2014;28:1059–65. https://doi.org/10.1021/ef401705g.
[31] Mao Y, Dong Y, Wang B, Chang J, Yu J, Zhang Y, et al. Characteristics and kinetics of biomass tar cracking in a micro fluidized bed. RSC Adv 2015;5:82845–52. https://doi.org/10.1039/C5RA13323H.
[32] Thimthong N, Appari S, Tanaka R, Iwanaga K, Kudo S, Hayashi J, et al. Kinetic modeling of non-catalytic partial oxidation of nascent volatiles derived from fast pyrolysis of woody biomass with detailed chemistry. Fuel Processing Technology 2015;134:159–67. https://doi.org/10.1016/j.fuproc.2015.01.029.
[33] Tanoh TS. Production d'un syngaz par pyrogazéification de biomasse en vur d'une biométhanation. Université de Toulouse, 2021.
[34] Dhahak A, Bounaceur R, Le Dreff-Lorimier C, Schmidt G, Trouve G, Battin-Leclerc F. Development of a detailed kinetic model for the combustion of biomass. Fuel 2019;242:756–74. https://doi.org/10.1016/j.fuel.2019.01.093.
[35] Norinaga K, Deutschmann O, Saegusa N, Hayashi J. Analysis of pyrolysis products from light hydrocarbons and kinetic modeling for growth of polycyclic aromatic hydrocarbons with detailed chemistry. Journal of Analytical and Applied Pyrolysis 2009;86:148–60. https://doi.org/10.1016/j.jaap.2009.05.001.
[36] Norinaga K, Shoji T, Kudo S, Hayashi J. Detailed chemical kinetic modelling of vapour-phase cracking of multi-component molecular mixtures derived from the fast pyrolysis of cellulose. Fuel 2013;103:141–50. https://doi.org/10.1016/j.fuel.2011.07.045.
[37] Srinivas S, Field RP, Herzog HJ. Modeling Tar Handling Options in Biomass Gasification. Energy Fuels 2013;27:2859–73. https://doi.org/10.1021/ef400388u.
[38] Ruiz M, Schnitzer A, Arnoux P, Mauviel G. Gasification of N-rich fibreboard in an air-blown fluidized bed reactor: A study on the fate of tars, NH3 and HCN during oxidative mild Hot Gas Filtration. Fuel 2021;303:121317. https://doi.org/10.1016/j.fuel.2021.121317.
[39] Kister J, Pieri N, Alvarez R, Díez MA, Pis JJ. Effects of Preheating and Oxidation on Two Bituminous Coals Assessed by Synchronous UV Fluorescence and FTIR Spectroscopy. Energy Fuels 1996;10:948–57. https://doi.org/10.1021/ef950159a.
[40] Lardier G, Kaknics J, Dufour A, Michel R, Cluet B, Authier O, et al. Gas and Bed Axial Composition in a Bubbling Fluidized Bed Gasifier: Results with Miscanthus and Olivine. Energy Fuels 2016;30:8316–26. https://doi.org/10.1021/acs.energyfuels.6b01816.
[41] Septien S, Valin S, Peyrot M, Spindler B, Salvador S. Influence of steam on gasification of millimetric wood particles in a drop tube reactor: Experiments and modelling. Fuel 2013;103:1080–9. https://doi.org/10.1016/j.fuel.2012.09.011.
[42] Darido J, Dhahak A, Bounaceur R, Le Dreff - Lorimier C, Leyssens G, Cazier F, et al. Emissions from a Domestic Wood Heating Appliance: Experimental Measurements and Numerical Study Using an Equivalent Reactor Network (ERN) Approach Coupled with a Detailed Chemical Mechanism. Energy Fuels 2021:acs.energyfuels.1c01927. https://doi.org/10.1021/acs.energyfuels.1c01927.
[43] Stagni A, Cuoci A, Frassoldati A, Faravelli T, Ranzi E. Lumping and Reduction of Detailed Kinetic Schemes: an Effective Coupling. Ind Eng Chem Res 2014;53:9004–16. https://doi.org/10.1021/ie403272f.
[44] Pejpichestakul W, Ranzi E, Pelucchi M, Frassoldati A, Cuoci A, Parente A, et al. Examination of a soot model in premixed laminar flames at fuel-rich conditions. Proceedings of the Combustion Institute 2019;37:1013–21. https://doi.org/10.1016/j.proci.2018.06.104.
[45] Saggese C, Sánchez NE, Frassoldati A, Cuoci A, Faravelli T, Alzueta MU, et al. Kinetic Modeling Study of Polycyclic Aromatic Hydrocarbons and Soot Formation in Acetylene Pyrolysis. Energy Fuels 2014;28:1489–501. https://doi.org/10.1021/ef402048q.

[46] Rabou LPLM, Zwart RWR, Vreugdenhil BJ, Bos L. Tar in Biomass Producer Gas, the Energy research Centre of The Netherlands (ECN) Experience: An Enduring Challenge. Energy Fuels 2009;23:6189–98. https://doi.org/10.1021/ef9007032.
[47] Valin S, Cances J, Castelli P, Thiery S, Dufour A, Boissonnet G, et al. Upgrading biomass pyrolysis gas by conversion of methane at high temperature: Experiments and modelling. Fuel 2009;88:834–42. https://doi.org/10.1016/j.fuel.2008.11.033.
[48] Demol R, Dufour A, Rogaume Y, Mauviel G. Production of Purified H2, Heat, and Biochar from Wood: Comparison between Gasification and Autothermal Pyrolysis Based on Advanced Process Modeling. Energy Fuels 2022;36:488–501. https://doi.org/10.1021/acs.energyfuels.1c03528.